Chapter 1

Novel Insight into Morphological Features and Vascular Profile of Selected Macular Dystrophies Using Swept-Source Optical Coherence Tomography and Optical Coherence Tomography Angiography

Magdy Moussa and Mahmoud Leila

Additional information is available at the end of the chapter

http://dx.doi.org/10.5772/intechopen.78679

Abstract

Our perception of macular dystrophies has evolved overtime from collective grouping into hereditary disorders of unclear etiology and no effective treatment to avid search for the underlying pathogenic mechanism that would provide base for future therapy. A causal conjunction between abnormalities in the photoreceptors layer and the RPE—Bruch's membrane complex and abnormal profile of the retinal vascular plexuses and the choriocapillaris—stands out as a plausible theory of pathogenesis. The recently introduced swept-source optical coherence tomography (SS-OCT) technology incorporates long-wavelength (1050-nm) scanning light, less susceptibility to sensitivity roll-off, and ultrahigh-speed image acquisition. These features enabled in vivo noninvasive visualization of different strata of the outer retina and the choriocapillaris with unprecedented finesse. Furthermore, the SS-OCT technology incorporated a blood flow detection algorithm; OCTARA that in tandem with the deeper penetration and superior axial resolution of SS-OCT enabled detailed assessment of the retinal capillary plexuses and the choriocapillaris in terms of structure and density. This novel technology could help explore yet undiscovered frontiers in the pathophysiology of macular dystrophies and guide future therapeutic approaches. This chapter includes a review of literature along with the authors' experience in imaging selected macular dystrophies using SS-OCT and SS-OCT angiography (SS-OCTA).

Keywords: imaging macular dystrophies, SS-OCTA in Stargardt's, SS-OCTA in Best's disease, OCTARA algorithm, swept-source OCT

1. Introduction

Macular dystrophy is a unifying term used to describe a group of hereditary fundus disorders that exhibits Mendelian inheritance pattern and has varying degrees of expressivity and penetrance. These disorders share common criteria in that they are isolated, that is, confined to the eye with no systemic association, limited to the anatomic macula, exhibit bilateral involvement with striking symmetry, and have characteristic biomicroscopic features that manifest universally along with visual symptoms or often discovered on routine examination before symptoms develop. The classic tools for the diagnosis and follow-up of macular dystrophies were largely based on clinical appearance, electrophysiologic findings, and fundus fluorescein angiography (FFA). More recently, fundus autofluorescence (FAF) increasingly became an invaluable noninvasive tool in the follow-up scheme of these patients [1–7]. FAF captures the stimulated emission of light from lipofuscin molecules that accumulate excessively in cases of retinal pigment epithelium (RPE) dysfunction and depicts specific autofluorescence patterns that are characteristic for each disease [8–11]. To date, there is no known effective treatment for macular dystrophies other than the management of complications, for example, choroidal neovascularization (CNV) secondary to Best's disease and visual rehabilitation using low-vision aids [1, 2].

2. Theories of pathogenesis of vascular changes in macular dystrophies

Histopathological studies in humans affected with macular dystrophies and in animal models of retinal degeneration demonstrated a wide-spread loss of the photoreceptors and the RPE, in addition to extensive vascular remodeling of the retinal vascular plexuses and the choriocapillaris [1, 2, 12]. These findings purported a cause–effect relationship between the morphological changes seen in retinal microstructure and the status of vascular nourishment, in the sense that one pathology is a consequence of the other, though the exact mechanism remains debatable [13–15]. One theory proposes that the progressive demise of photoreceptors and RPE causes a thinning out of the retina with subsequent progressive atrophy of retinal vasculature and choriocapillaris as part of a downregulation process due to a reduced vascular demand [16]. Another proposed mechanism is that retinal thinning due to the loss of photoreceptors and RPE allows more oxygen influx into the inner retinal layers from the choroidal circulation. The ensuing retinal hyperoxic state induces vasoconstriction and vascular rarefaction [12]. Another plausible theory is that progressive RPE loss results in a decreased release of vascular endothelial growth factor (VEGF) and other signaling factors that are essential for the viability of the choriocapillaris, hence precipitating choriocapillaris atrophy [17–19]. Finally, some researches propose that mechanical compression by the lipofuscin-laden RPE and accumulation of hyaline deposits between the RPE and Bruch's membrane exerts mechanical compression on the choriocapillaris with subsequent atrophy and loss [16].

http://dx.doi.org/10.5772/intechopen.78679

3. Optical coherence tomography angiography (OCTA): a new imaging frontier

The prospect of an abnormal vascular profile going on in tandem with the morphological changes in retinal microstructure in macular dystrophies turned our attention to the diagnostic and therapeutic potentials of the early detection of abnormal changes in the retinal vascular plexuses and the choriocapillaris. Currently, the available diagnostic modalities rely on inference extrapolated from indirect evidence to determine disease stage and progression. For instance, FFA depicts disease patterns based on varying degrees of fluorescence; FAF identifies diseased or dead RPE cells based on varying intensities of lipofuscin autofluorescence, whereas electrophysiology records the amplitude and latency of electric transduction in retinal layers to identify different dystrophies [1–3, 8–11]. The common factor among these diagnostic tools is that they reveal useful information only when retinal function due to a given dystrophy has already been compromised. In comparison, OCTA offers direct noninvasive visualization of the vascular profile in macular dystrophies and thus has the clear advantages of screening vulnerable population and detecting the disease process in its nascence. Though no therapeutic line is currently available for macular dystrophies, the identification of early disease phases based on the integrity of the vascular profile helps selecting patients who would be best candidates for on-going research trials on gene therapy and pluripotent stem cell transplantation. On the other hand, identifying patients with severely compromised vascular profile, and in whom favorable outcome of these therapies is unlikely, will help avoid biased results and reduce the economic burden on health-care institutions.

4. Swept-source optical coherence tomography (SS-OCT), SS-OCT angiography (SS-OCTA), and OCTARA algorithm

SS-OCTA incorporates a blood flow detection algorithm; OCTARA (Optical Coherence Tomography Angiography Ratio Analysis); Topcon Corporation, Tokyo, Japan. OCTARA uses decorrelation motion contrast between rapidly repeated SS-OCT B-scans to detect moving erythrocytes in relation to static tissue [20]. SS-OCTA is integrated in the SS-OCT technology which incorporates a long-wavelength (1050-nm) scanning light, reduced sensitivity roll-off feature, and ultrahigh-speed image acquisition. These implements enable deeper penetration with minimal light scattering, hence superior axial resolution and segmentation of different retinal layers. The result is the generation of ultrahigh-definition images of the retinal microstructure, retinal vascular plexuses, and the choriocapillaris, while obviating the need for dye injection. It is worth noting that OCTARA algorithm generates SS-OCTA images by registering B-scan repetition at each scan location, thereby computing a ratio-based result between corresponding image pixels. This method preserves the integrity of the OCT spectrum and does not result in compromised axial resolution, an inherent disadvantage of other OCTA technologies [20–25]. In addition, SS-OCTA software generates color-coded flow density maps of the retinal vascular plexuses and the choriocapillaris, each layer separately.

In this map, vessel density in a given area is inferred from the decorrelation motion contrast signal provided by SS-OCTA, where high flow is represented by an increased vessel density and vice versa. Different vessel densities are then given color codes and numeric percentage values that reflect the percentage area occupied by blood vessels, where bright red color represents areas of highest density and hence a high numeric percentage, whereas dark blue represents areas of no detectable vessels and hence low or zero numeric percentage. Intermediate color shades represent variable grades of vessel density [26, 27].

5. SS-OCTA depiction of retinal vascular plexuses and the choriocapillaris in normal individuals

Normally, the retinal superficial capillary plexus (SCP) appears on SS-OCTA as an interlacing network of horizontal arterioles and venules connected by transverse capillaries and anastomosing together to form the peri-foveal capillary circle. Arterioles are surrounded by a wider capillary-free zone compared to venules. The retinal deep capillary plexus (DCP) appears as polygonal lobules or vortices composed of capillaries converging radially on an epicenter. The choriocapillaris appears as a homogeneous hyperintense layer composed of densely packed capillaries with no intervening dark spaces [21, 27, 28].

6. Spectral domain OCT (SD-OCT) and OCTA features of selected macular dystrophies

6.1. Stargardt's disease

Stargardt's disease is considered the most common inherited childhood dystrophy. The pattern of inheritance is an autosomal-recessive one and represents the mildest form of ABCA4 gene mutation. The mutated gene causes malfunction of the ATP-binding cassette proteins that have key role in cell transport processes within the photoreceptors layer. The resultant disruption of photoreceptors visual cycle leads to over-accumulation of a metabolic byproduct, namely lipofuscin in the RPE cell layer. Clinically, patients present with bilateral and symmetrical involvement of the posterior pole by characteristic yellowish flecks at the level of the RPE resembling fish scales. Occasionally, two adjacent flecks join in an obtuse angle reminiscent of a fish tail, hence the term pisciform. The end stage is characterized by resorption of flecks and ensuing atrophic maculopathy with a substantial visual loss. To date, no known treatment exists for Stargardt's disease [1, 2].

SD-OCT in Stargardt's disease demonstrates thinning of the outer retina including the photoreceptor layer and the RPE, and altered choroidal morphology in which the normal bowl-shaped contour of the choroidoscleral interface, with maximum thickness at the sub-foveal area, is replaced by an abnormal S-shaped contour due to a marked reduction of sub-foveal choroidal thickness and displacement of the thickest point of the choroid away from the

fovea [13]. On the other hand, OCTA imaging reveals generalized attenuation of the vascular layers of the ocular fundus, though the most significant vascular changes are located in the choriocapillaris, which exhibit generalized loss of the normal homogeneous hyperintense texture with the development of vascular rarefaction and flow-void areas. These morphological changes are attributed to the patchy loss of choriocapillaris or to the masking effect of the pisciform flecks [15, 29]. In some cases, there is enhanced visualization of the underlying Sattler's layer [16]. In terms of retinal capillary plexuses, vascular alterations of the SCP layer include rarefaction of the peri-foveal arcade with the enlargement of the foveal avascular zone (FAZ), and generalized reduction of vessel density in the SCP and the DCP layers, though these changes are most pronounced in the DCP layer [15, 28, 29].

6.2. Best's disease (vitelliform macular dystrophy)

Best's disease is an autosomal-dominant disorder whose primary target tissue is the RPE cell layer. The condition is caused by mutation in the BEST1 gene which causes the production of abnormal bestrophin protein. Normally located in the RPE plasma membrane, bestrophin acts as a calcium-dependent chloride channel and is responsible for normal ionic conduction across the RPE cell. Abnormal bestrophin formation causes the disruption of the ionic conduction within the RPE and interferes with the normal calcium metabolism that is essential for adhesiveness between interphotoreceptor matrix and the RPE layer. The end result is the deposition of abnormal amorphous vitelliform or egg yolk-like material in the photoreceptors' outer segments, within the RPE and sub-RPE. Though considered the hallmark of Best's disease, the origin of the vitelliform material remains uncertain. One plausible theory is that it is derived from the accumulation of lipofuscin material within over-shed photoreceptors' outer segments due to abnormal phagocytosis by RPE cell layer. Clinically, the disease is characterized by a solitary sub-retinal vitelliform lesion occupying the macular area. Less commonly, lesions may be multiple or eccentric in location. With time, the vitelliform lesion undergoes degeneration and may even get resorbed completely, with ensuing atrophic changes and scarring. Vision remains unaffected in early stages with most individuals maintaining reading and driving vision well into adult life until the atrophic or cicatricial stages develop. The abnormal ionic conduction in Best's disease is responsible for the characteristic loss of light response and abnormal Arden ratio on electro-oculogram (EOG) examination [1, 2].

SD-OCT in early stages of the disease shows a sub-retinal smooth dome-shaped amorphous optically opaque material. As the disease progresses, degenerative changes ensue on the vitelliform structure causing it to break down. The corresponding SD-OCT features consist of irregular optically—opaque amorphous deposits alternating with optically—translucent areas that correspond to the resorbed vitelliform material. In addition, RPE irregularities could be detected including irregular thickened RPE layer, and solitary or multiple RPE detachment(s) (PED). The atrophic stage of the disease is marked by diffuse disruption of the outer retinal layers including the external limiting membrane (ELM), inner segment/outer segment (IS/OS) photoreceptor junction, and marked atrophy or even disappearance of RPE cell layer [30, 31].

OCTA in Best's disease demonstrates generalized rarefaction of the SCP and the DCP layers along with a reduced vessel density. The mechanism of vascular rarefaction in Best's

disease is controversial. One explanation is that the vitelliform material causes centrifugal displacement of blood vessels in the macular area with resultant progressive atrophy due to mechanical compression. Occasionally, the DCP layer shows a central area of hypointense signal caused by vascular rarefaction and a reduced vessel density surrounded by an annulus of hyperintense signal. This peculiar configuration could be due to overcrowding of vessels being displaced by the vitelliform lesion, or due to compensatory dilatation of the para-macular vascular bed secondary to vessel rarefaction in the macula, with consequent increased blood flow. Likewise, the choriocapillaris shows vascular rarefaction with multiple hypointense flow-void areas, which could be explained by vascular impairment due to degenerative changes induced by mechanical compression or due to masking effect by the accumulating vitelliform material [30–35].

6.3. Choroidal neovascularization secondary to Best's disease: a diagnostic predicament

The most dreadful complication of Best's disease is CNV formation, which could develop in some cases secondary to compromised RPE/Bruch's complex [30, 32–34]. The advent of CNV on top of Best's disease could pose a diagnostic challenge due to overlapping fluorescein patterns of the vitelliform material and PEDs in Best's disease and the fibrovascular and neovascular components of CNV. Likewise, SD-OCT could yield inconclusive results, even when deploying the ultrahigh-definition versions, due to similar backscattering light intensity properties between the amorphous vitelliform and the CNV. OCTA helps disentangle this overlap by its ability to separate erythrocytes from the surrounding static tissue, hence displaying flow in a vascular network that is pathognomonic of CVN formation. In addition, OCTA integrates light-scattering reduction technology (reduced sensitivity roll-off) that preserves the integrity of the incident infra-red laser beam, hence allowing deeper penetration, layer segmentation, and delineation of the neovascular network of CNV from the surrounding vitelliform material [20, 27, 36–40].

7. Authors' case reports

Over the past year, the authors studied 40 patients with macular dystrophies (27 patients with Best's disease and adult-onset vitelliform foveomacular dystrophy, and 13 patients with Stargardt's disease). SS-OCT and SS-OCTA images were acquired using the DRI OCT Triton machine version 10.11 (Topcon Corporation, Tokyo, Japan). Herein, we present representative cases to demonstrate our findings regarding the morphological alteration in retinal microstructure, retinal vascular plexuses, and choriocapillaris in different stages of both diseases.

7.1. SS-OCT and SS-OCTA findings in Stargardt's disease

Case 1. Early stage of Stargardt's disease. A 26-year-old male presented with defective vision in both eyes of approximately 1-year duration. His best-corrected visual acuity (BCVA) was 20/63 and 20/50 in the right eye (RE) and the left eye (LE), respectively. Fundus examination

revealed bilateral numerous yellowish discrete flecks in the macular area at the level of the RPE. The lesions were identical in appearance though more numerous in the RE. SS-OCT examination revealed bilateral foveal thinning, disrupted ELM and IS/OS photoreceptor junction, and thinning of the choriocapillaris with enhanced visualization of the larger choroidal vessels. SS-OCTA revealed bilateral rarefaction of the SCP and the DCP layers. Affection was more pronounced in the DCP layer. The choriocapillaris showed a moth-eaten appearance instead of the normal hyperintense homogeneous texture, due to the presence of multiple black areas that could correspond to areas of flow void or masking effect by the pisciform lesions. The corresponding flow density maps showed a reduced vessel density that corresponded to vascular rarefaction in the SCP, the DCP, and the choriocapillaris (**Figures 1** and **2**).

Case 2. Late stage of Stargardt's disease. A 58-year-old female who was a known case of Stargardt's disease presented for follow-up with complaints of defective vision in both eyes of approximately 2-year duration. Her BCVA was 20/400 and 20/200 in the RE and the LE, respectively. Fundus examination of the RE revealed a sharply circumscribed area of geographic atrophy occupying the macula, approximately of 4 disc diameters (DD) in size. On

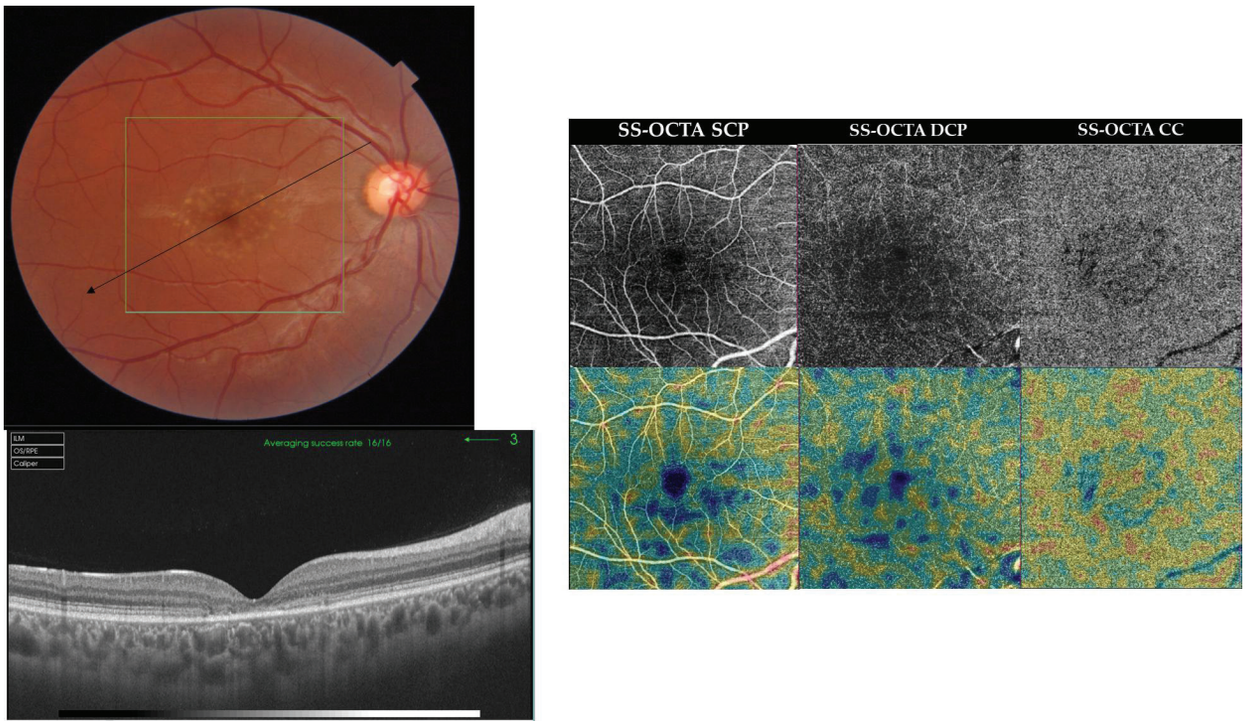

Figure 1. Case 1. Top left, color photograph of the RE of a 26-year-old male in early stage of Stargardt's disease. Note the numerous subretinal pisciform yellowish flecks occupying the macular area. Bottom left, radial scan SS-OCT shows foveal thinning (168 μ), disrupted ELM and IS/OS photoreceptor junction, and thinning of the choriocapillaris with enhanced visualization of the larger choroidal vessels. Right, en face SS-OCTA projection of the SCP, the DCP, and the choriocapillaris in a 6 × 6 mm field (upper row), and the corresponding flow density maps (lower row). The SCP and the DCP layers show vascular rarefaction. Affection is more pronounced in the DCP layer. The choriocapillaris shows a moth-eaten appearance instead of the normal homogeneous hyperintense texture, due to the presence of multiple black areas of flow voids. The corresponding flow density maps show a reduced vessel density that corresponds to vascular rarefaction in the SCP, the DCP, and the choriocapillaris.

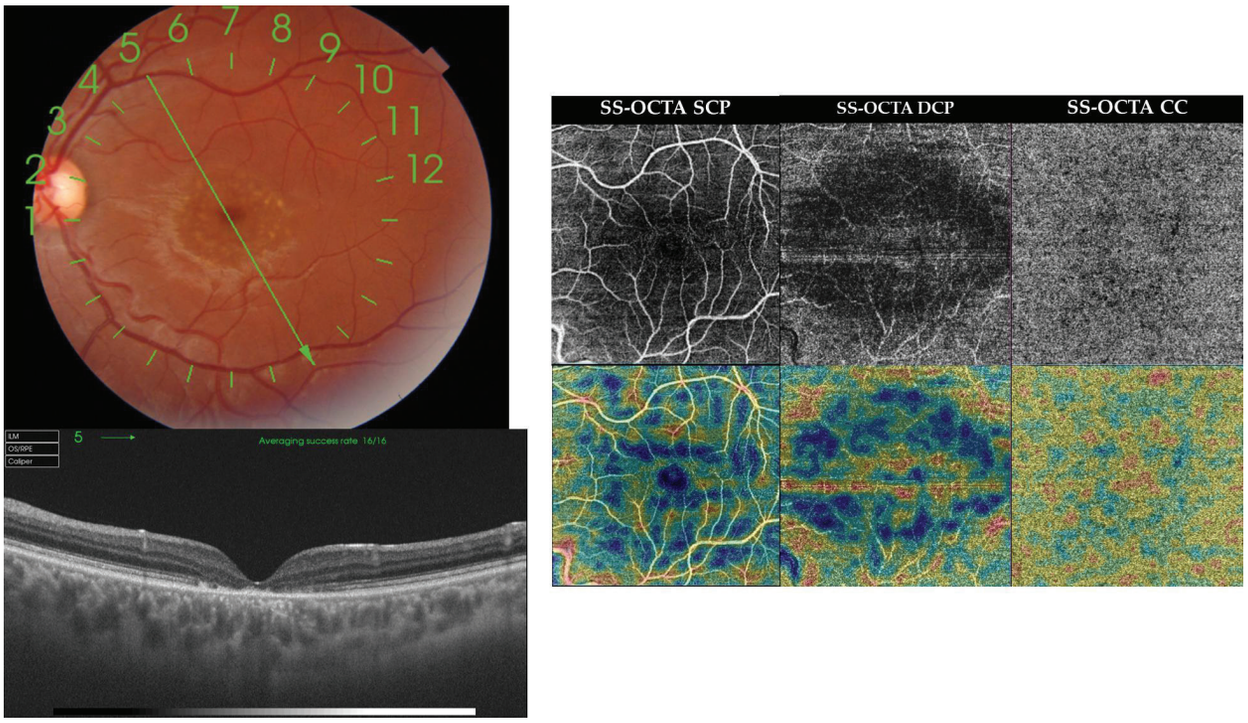

Figure 2. Case 1. Top left, color photograph of the LE of the same patient as in **Figure 1**. The fundus shows identical lesions to those seen in the RE though less numerous. Bottom left, radial scan SS-OCT reveals foveal thinning (144 μ), disrupted ELM and IS/OS photoreceptors junction, and thinning of the choriocapillaris with enhanced visualization of the larger choroidal vessels. Right, en face SS-OCTA projection of the SCP, the DCP, and the choriocapillaris in a 6 × 6 mm field (upper row), and the corresponding flow density maps (lower row). The SCP and the DCP layers demonstrate vascular rarefaction. Affection is more pronounced in the DCP layer. The choriocapillaris shows multiple black areas of flow voids. The corresponding flow density maps show a reduced vessel density that corresponds to vascular rarefaction in the SCP, the DCP, and the choriocapillaris.

FFA, the lesion seen in the color photograph demonstrated that the RPE in the center of the lesion has virtually disappeared with unveiling of the underlying large choroidal vessels. More peripheral areas of the lesion demonstrated transmission fluorescence. SS-OCT of the same eye showed foveal thinning, wiping-out of the ELM, and the IS/OS layer in the subfoveal area. The RPE layer was extremely rarified with extensive loss of the choriocapillaris and enhanced visualization of the underlying choroidal vessels. SS-OCTA of the SCP and the DCP layers of the same eye showed vascular rarefaction and reduced vessel density. These changes were most pronounced in the DCP layer. SS-OCTA at the level of the choriocapillaris showed complete loss of the vessels in the central portion of the lesion with clear view of the larger choroidal vessels. This peculiar configuration could be explained by severe atrophy of the choriocapillaris and Sattler's layer, and visualization of an anteriorly displaced Haller's layer to the level of the choriocapillaris. The central region was surrounded by an annulus of hypointense flow-void areas and vessel rarefaction (arrows). The LE had a similar lesion though slightly smaller in size (3DD) and less advanced in terms of the extent of geographic atrophy. SS-OCT of the same eye showed fairly preserved ELM though disrupted IS/OS layer and marked RPE thinning. The diffuse atrophy of the choriocapillaris resulted in irregular thickening of the choroid with loss of the normal bowl-shaped configuration of

http://dx.doi.org/10.5772/intechopen.78679

the choroidoscleral junction. SS-OCTA of the LE reflected the relatively less advance disease compared to the RE, especially in the choriocapillaris layer which showed multiple flow-void areas but with less diffuse atrophy than noted in the RE (**Figures 3** and **4**).

7.2. SS-OCT and SS-OCTA findings in Best's disease and adult-onset vitelliform foveomacular dystrophy

Case 3. Adult-onset vitelliform foveomacular dystrophy. A 61-year-old female presented with defective vision in the RE of approximately 6-month duration. Her BCVA was 20/100 and 20/400 in the RE and the LE, respectively. Fundus examination of the RE revealed a sub-foveal plaque of amorphous yellowish-white material surrounded by numerous satellite lesions varying in size and in shape, and scattered in the anatomic macula region. On the corresponding FFA, the sub-foveal lesion showed blocked hypofluorescence with multiple pin-point hyperfluorescent spots due to leakage within PED. The satellite lesions seen in the color

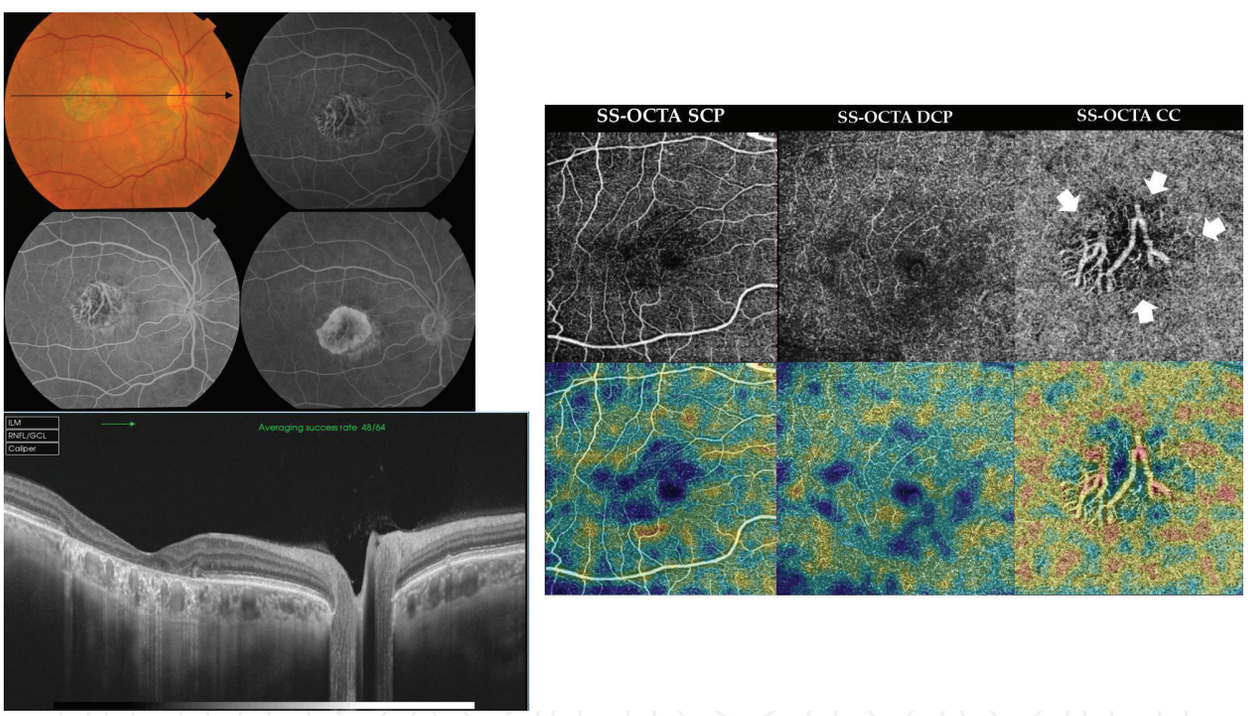

Figure 3. Case 2. Top left, color photograph and FFA of the RE of a 58-year-old female in late stage of Stargardt's disease. The fundus shows a sharply circumscribed area of geographic atrophy occupying the macula, approximately 4 DD in size. On FFA, the RPE in the center of the lesion has virtually disappeared with unveiling of the large choroidal vessels. More peripheral areas of the lesion demonstrated transmission fluorescence. Bottom left, high-definition line scan (12.0 mm) SS-OCT of the same eye shows marked foveal thinning (84 μ), wiping out of the ELM and the IS/OS layer in the sub-foveal area. The RPE layer is extremely rarified with extensive loss of the choriocapillaris and enhanced visualization of the underlying choroidal vessels. Right, en face SS-OCTA projection of the SCP, the DCP, and the choriocapillaris in a 6 × 6 mm field (upper row), and the corresponding flow density maps (lower row). The SCP and the DCP layers show vascular rarefaction and reduced vessel density. These changes are most pronounced in the DCP layer. The choriocapillaris shows complete loss of vessels in the central portion of the lesion with clear view of the larger choroidal vessels. The central region is surrounded by an annulus of hypointense flow-void areas and vessel rarefaction (arrows).

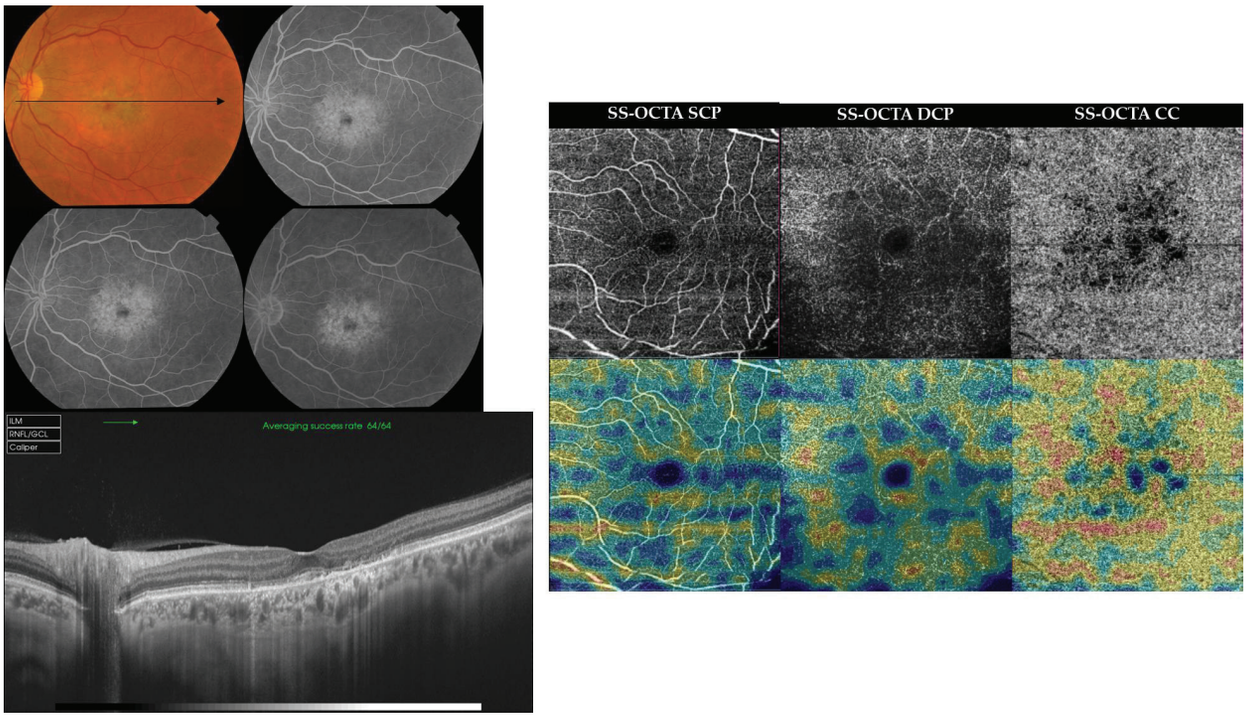

Figure 4. Case 2. Top left, color photograph and FFA of the LE of the same patient as in **Figure 3**. The fundus shows a sharply circumscribed area of geographic atrophy occupying the macula, approximately 3 DD in size. FFA in the macular area demonstrated transmission fluorescence due to marked RPE attenuation. Bottom left, high-definition line scan (12.0 mm) SS-OCT of the same eye shows foveal thinning (177 μ), wiping out of the IS/OS layer in the sub foveal area. The RPE layer was extremely rarified with extensive loss of the choriocapillaris and enhanced visualization of the underlying choroidal vessels. The diffuse atrophy of the choriocapillaris resulted in irregular thickening of the choroid with loss of the normal bowl-shaped configuration of the choroidoscleral junction. Sub-foveal choroidal thickness is 257 μ. Right, en face SS-OCTA projection of the SCP, the DCP, and the choriocapillaris in a 6 × 6 mm field (upper row), and the corresponding flow density maps (lower row). The SCP and the DCP layers show vascular rarefaction and reduced vessel density. These changes are most pronounced in the DCP layer. The choriocapillaris shows vascular rarefaction with development of multiple hypointense flow-void areas.

photograph demonstrated hyperfluorescence caused by a combination of staining, pooling in PED, and transmission fluorescence due to RPE atrophy. SS-OCT of the same eye showed a dome-shaped hyper-reflective sub-foveal lesion corresponding to the yellowish vitelliform deposits seen in the color fundus photograph. The entire lesion was optically opaque except for a small optically lucent area caused by breakdown of the vitelliform material. The underlying RPE was thickened and irregular with multiple PED formation and marked thinning of the underlying choriocapillaris. SS-OCTA of the SCP layer was essentially normal in appearance apart from irregularity of the FAZ (arrow) and scattered flow-void areas (circles). The DCP layer showed centrifugal displacement of the peri-foveal vessels with extensive vascular rarefaction and enlargement of the FAZ (arrows). The para-foveal area showed hyperintense signal derived from abnormally high flow within the overcrowded vessels due to lateral displacement by the vitelliform material (asterisk). The choriocapillaris showed patchy hypointense areas that corresponded to the abovementioned vitelliform lesions. The hypointense signal might represent flow-void areas due to choriocapillaris atrophy or due to masking by the vitelliform material. The LE had rather similar fundus changes though FFA revealed more extensive RPE atrophy (**Figures 5** and **6**).

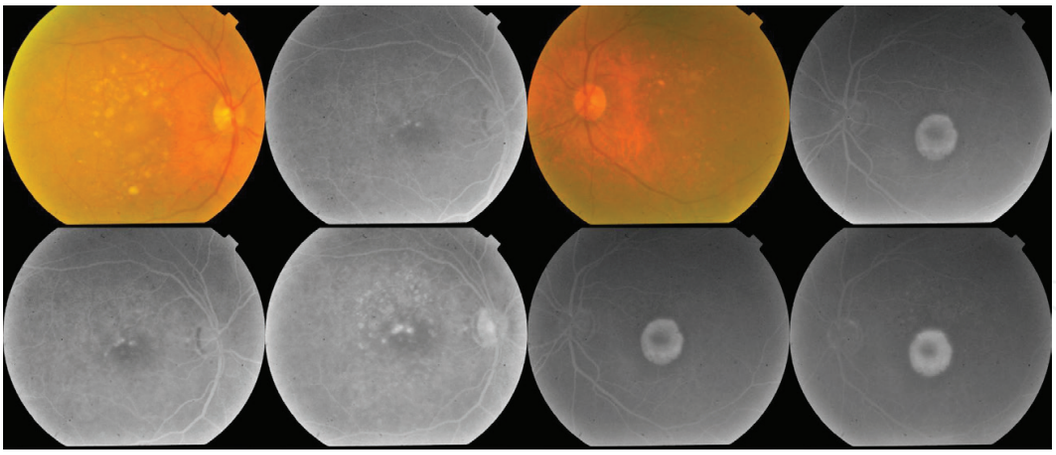

Figure 5. Case 3. Color photograph and FFA of the RE and the LE of a 61-year-old female in the vitelliruptive stage of Best's disease. The fundus of the RE shows a sub-foveal plaque of amorphous yellowish-white material surrounded by numerous satellite lesions varying in size and shape, and scattered in the anatomic macula. On the corresponding FFA, the sub-foveal lesion shows blocked hypofluorescence with multiple pin-point hyperfluorescent spots due to leakage within PED. The satellite lesions seen in the color photograph demonstrate hyperfluorescence caused by a combination of staining, pooling in PED, and transmission fluorescence due to RPE atrophy. The LE had rather similar fundus changes though FFA revealed more extensive RPE atrophy.

Case 4. Cicatricial stage of Best's disease. A 30-year-old female presented with defective vision in both eyes of 3–6 months duration. Her BCVA was 20/80 and 20/100 in the RE and the LE, respectively. Fundus examination of the LE revealed a sub-foveal sharply circumscribed ovoid area of RPE changes with central scarring. The lesion measured approximately 1 DD. On the corresponding FFA, the lesion seen in the color photograph demonstrated transmitted fluorescence due to RPE attenuation with late staining of scar tissue. The RPE in the center of the lesion has virtually disappeared with unveiling of the large choroidal vessels in earlier phases of the angiogram. SS-OCT of the same eye showed marked thinning of the fovea with a hyper-reflective scar tissue replacing the sub-foveal outer retinal layers, the choriocapillaris, and extending well into the underlying choroid. The immediate para-foveal area showed a sub-retinal pouch of optically lucent space with optically opaque sub-retinal clumps representative of degenerative changes peculiar of an earlier vitelliruptive stage. SS-OCTA of the DCP layer showed extensive vascular rarefaction in the area previously occupied by the vitelliform material. The choriocapillaris shows a central hypointense flow-void area surrounded by an outer zone of vascular rarefaction. The RE had rather similar fundus changes. The corresponding FFA revealed foveal RPE atrophy with on outer rim of blocked fluorescence due to RPE hyperplasia (**Figures 7** and **8**).

Case 5. CNV complicating cicatricial stage of Best's disease. A 28-year-old female complaining of recent diminution of vision in the RE 10 days ago. Her BCVA was 20/80 and 20/400 in the RE and the LE, respectively. Fundus examination of the RE showed an area of shallow neurosensory detachment in the foveal region, approximately 1.5 DD. The lesion showed yellowish-white precipitates gravitating in its inferior portion. On FFA, the lesion seen in the color photograph demonstrated early well-defined disc-shaped hyperfluorescence inferiorly with progressively increasing fluorescence intensity suggestive of classic CNV formation. The lesion was surrounded by diffuse and fuzzy hyperfluorescence due to pooling in

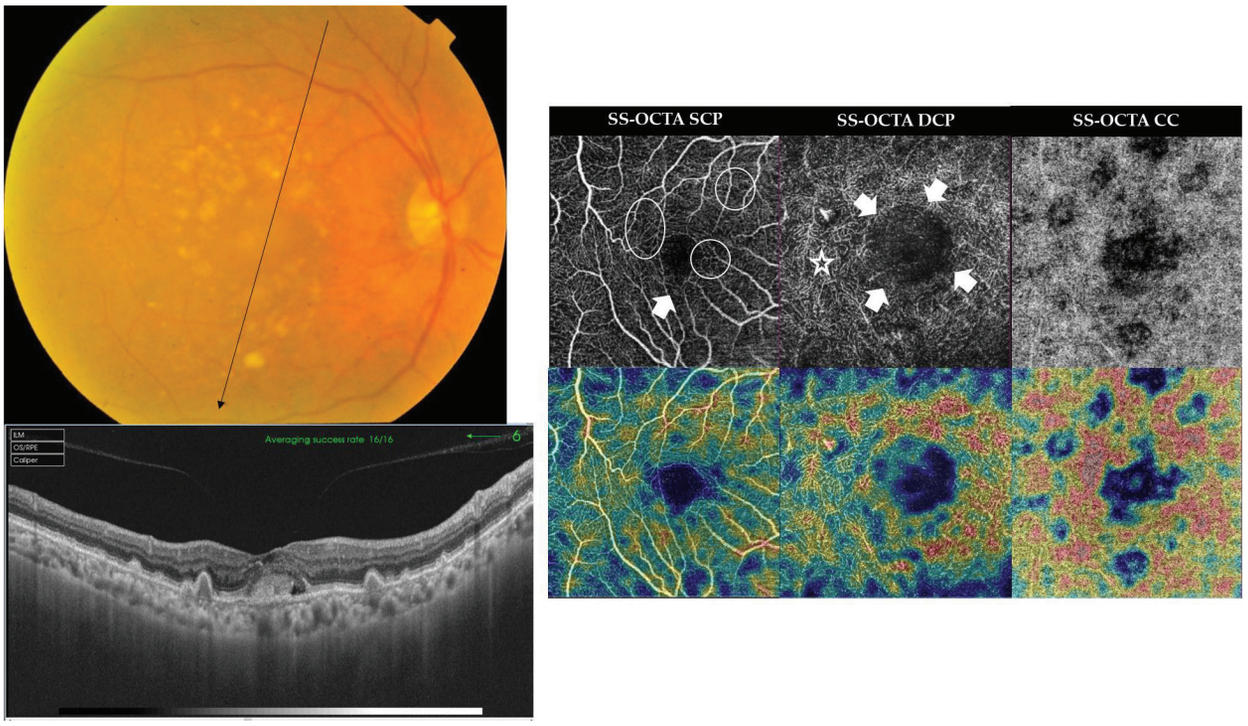

Figure 6. Case 3. Left, radial scan SS-OCT of the RE of the same patient as in **Figure 5**. Note the dome-shaped hyperreflective sub-foveal lesion. The entire lesion is optically opaque except for a small optically lucent area caused by breakdown of the vitelliform material. The underlying RPE is thickened and irregular with multiple PED formation and marked thinning of the underlying choriocapillaris. Sub-foveal choroidal thickness measured 159 μ. Right, en face SS-OCTA projection of the SCP, the DCP, and the choriocapillaris in a 4.5 × 4.5 mm field (upper row), and the corresponding flow density maps (lower row). The SCP layer is essentially normal in appearance apart from irregularity of the FAZ (arrow) and scattered flow-void areas (circles). The DCP layer shows centrifugal displacement of the perifoveal vessels with extensive vascular rarefaction and enlargement of the FAZ (arrows). Note the hyperintense signal derived from abnormally high flow within overcrowded vessels in the para-foveal area (asterisk). The choriocapillaris shows patchy hypointense flow-void areas that corresponded to the location of the abovementioned vitelliform lesions.

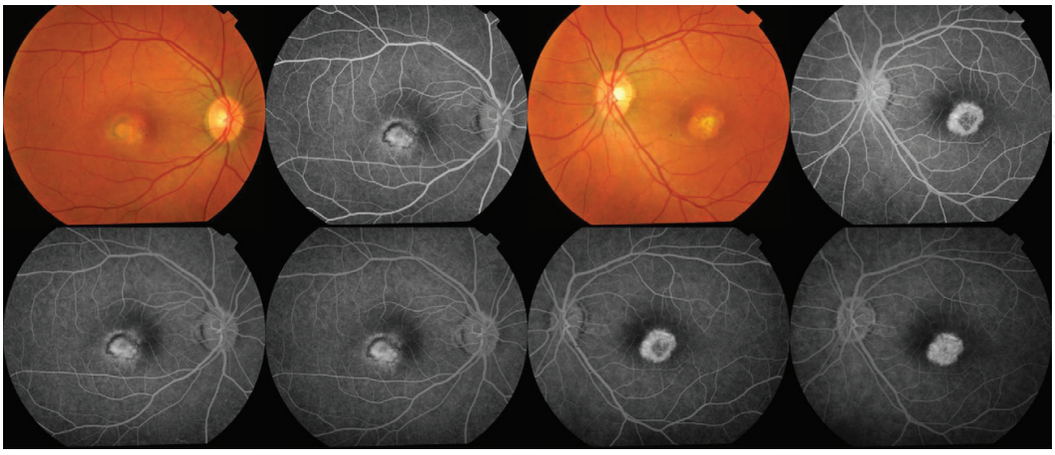

Figure 7. Case 4. Color photograph and FFA of the RE and the LE of a 30-year-old female in the cicatricial stage of Best's disease. The fundus of the LE reveals a sub-foveal sharply circumscribed ovoid area of RPE changes with central scarring. The lesion measures approximately 1 DD. On the corresponding FFA, the lesion demonstrates transmitted fluorescence due to RPE attenuation with late staining of scar tissue. The RPE in the center of the lesion has virtually disappeared with unveiling of the large choroidal vessels in earlier phases of the angiogram. The RE shows rather similar fundus changes. The corresponding FFA reveals foveal RPE atrophy with an outer rim of blocked fluorescence due to RPE hyperplasia.

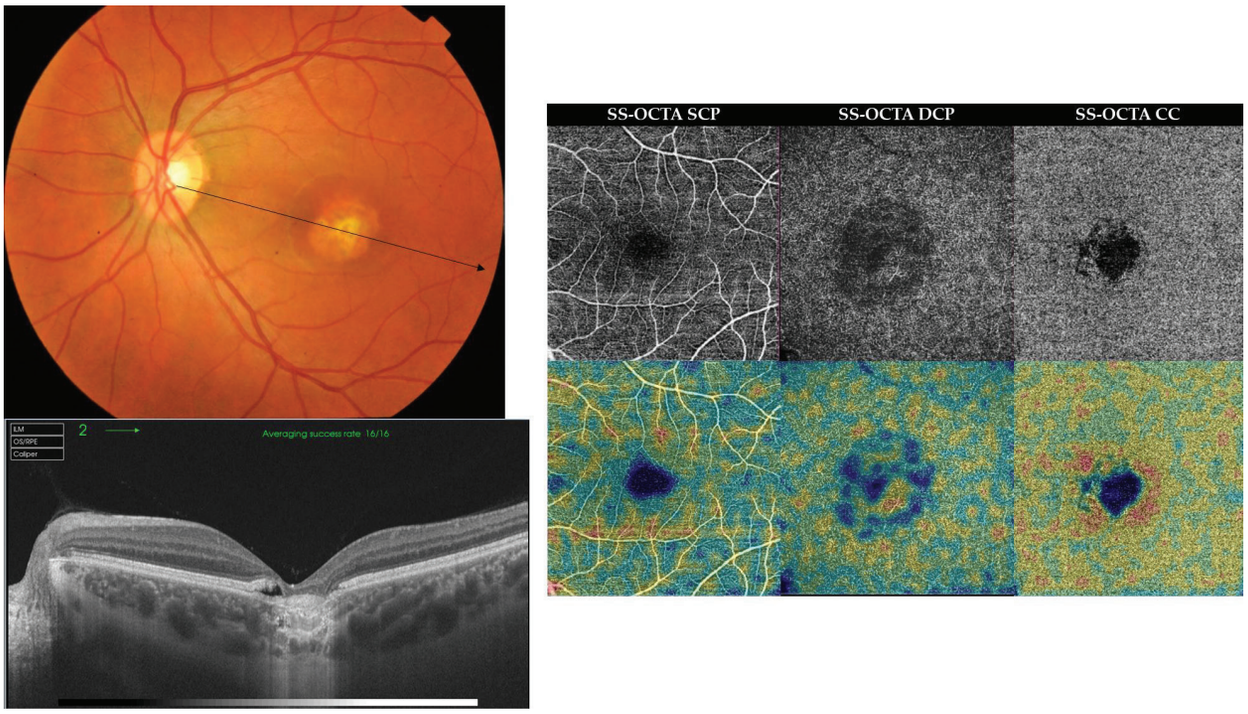

Figure 8. Case 4. Left, radial scan SS-OCT of the LE of the same patient as in **Figure 7**. Note marked thinning of the fovea with a hyper-reflective scar tissue replacing the sub-foveal outer retinal layers, the choriocapillaris, and extending well into the underlying choroid. Right, en face SS-OCTA projection of the SCP, the DCP, and the choriocapillaris in a 6 × 6 mm field (upper row), and the corresponding flow density maps (lower row). The DCP layer shows extensive vascular rarefaction in the area previously occupied by the vitelliform material. The choriocapillaris shows a central hypointense flow-void area surrounded by an outer zone of vascular rarefaction.

the neurosensory detachment cavity. An inferior rim of transmission fluorescence is noted. SS-OCT of the same eye showed sub-foveal shallow neurosensory detachment with hyper-reflective amorphous lesion, along with disrupted outer retinal layers and marked atrophy of the RPE. SS-OCTA of the DCP layer showed vascular rarefaction in the area previously occupied by the vitelliform material. The normally avascular outer retina showed a para-central hyperintense signal characteristic of active CNV formation. The LE had a macular scar with corresponding transmission fluorescence on FFA (**Figures 9** and **10**).

Case 6. CNV complicating cicatricial stage of Best's disease. A 9-year-old male presented to our clinic complaining of recent diminution of vision in the RE of few days duration. The patient was a known case of Best's disease. His BCVA was 20/200 and 20/400 in the RE and the LE, respectively. Fundus biomicroscopy examination of both eyes showed the typical scrambled-egg lesion occupying the macular area. The lesion was surrounded by residual neurosensory detachment and showed inferior migration of yellowish material and RPE alteration. The entire lesion measured approximately 2 DD in size. In the RE, the inferior portion of the scrambled-egg lesion was surrounded by a ring of deep retinal hemorrhage. FFA of both eyes demonstrated stippled fluorescence pattern due to RPE alteration, late staining of the yellowish material, and pooling of the dye in the neurosensory detachment but without conclusive evidence of CNV formation. SS-OCT of both eyes showed the typical dome-shaped hyper-reflective lesion at the level of RPE extending into—and surrounded by—empty sub-retinal space. On the other hand, SS-OCTA of the RE at the plane of the outer retina demonstrated

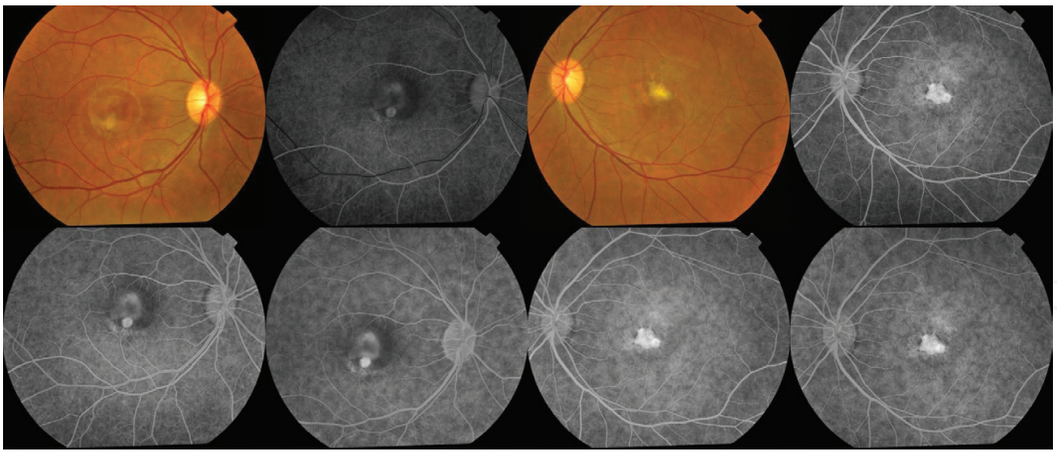

Figure 9. Case 5. Color photograph and FFA of the RE and the LE of a 28-year-old female with CNV secondary to cicatricial stage of Best's disease. The fundus of the RE shows an area of shallow neurosensory detachment in the foveal region, approximately 1.5 DD. The lesion shows yellowish-white precipitates gravitating in its inferior portion. The corresponding FFA demonstrates early well-defined disc-shaped hyperfluorescence inferiorly with progressively increasing fluorescence intensity suggestive of classic CNV. The LE had a macular scar with corresponding transmission fluorescence on FFA.

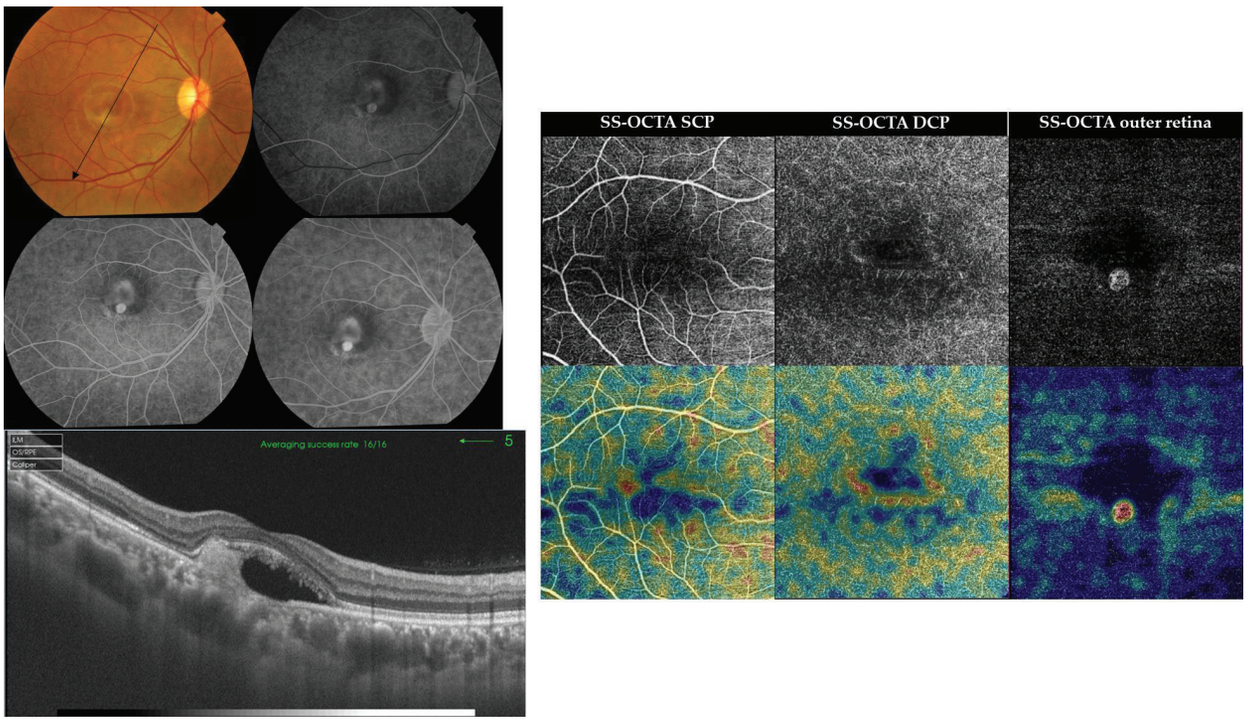

Figure 10. Case 5. Left, radial scan SS-OCT of the RE of the same patient as in **Figure 9**. Note the sub-foveal shallow neurosensory detachment with hyper-reflective amorphous lesion, along with disrupted outer retinal layers and marked atrophy of the RPE. Right, en face SS-OCTA projection of the SCP, the DCP, and the outer retina in a 6 × 6 mm field (upper row), and the corresponding flow density maps (lower row). The DCP layer shows vascular rarefaction in the area previously occupied by the vitelliform material. The outer retina shows a Para-central hyperintense signal characteristic of active CNV formation.

http://dx.doi.org/10.5772/intechopen.78679

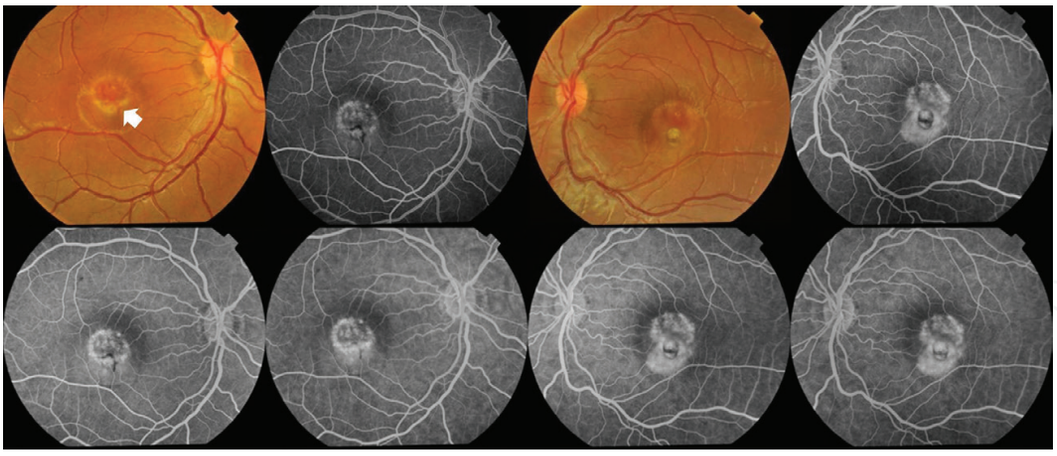

Figure 11. Case 6. Left, color fundus photograph and FFA of the RE shows a scrambled-egg lesion of vitelliform macular dystrophy surrounded by residual neurosensory detachment. The entire lesion measures approximately 2 DD in size. Note the inferior migration of the yellowish material with a ring of deep retinal hemorrhage (arrow). The corresponding FFA in arteriovenous phase of the same eye shows early transmitted fluorescence corresponding to RPE mottling seen in color photograph. Late phases of FFA show staining of the scrambled-egg lesion and residual sub-retinal yellowish deposits. Note the late pooling of the dye into the neurosensory detachment seen at the inferior edge of the vitelliform lesion. Right, color fundus photograph and FFA of the LE show essentially similar features to the RE.

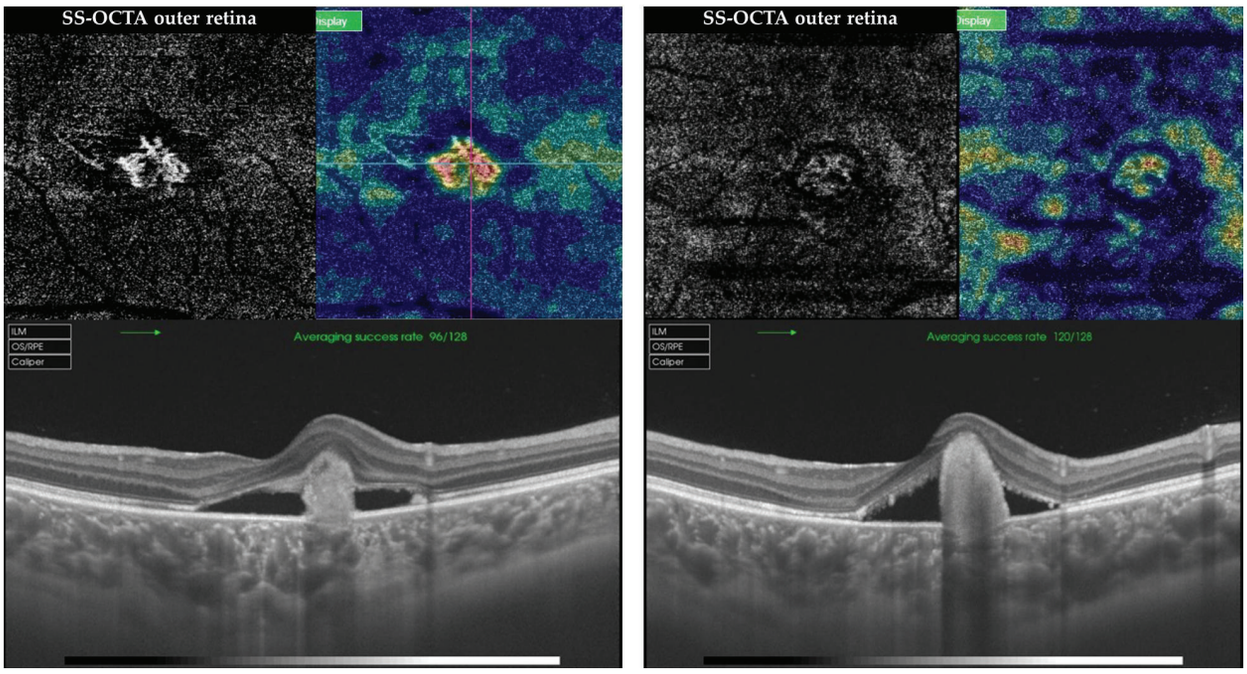

Figure 12. Case 6. Left, en face SS-OCTA projection of the outer retina and the corresponding flow density map in a 3 × 3 mm field of the RE of the same patient as in **Figure 11**. Note the hyperintense signal due to high flow within an interlacing curvilinear neovascular tuft characteristic of active CNV. Note the bright red color code denoting high vessel density. Corresponding SS-OCT shows the hyper-reflective lesion in the sub-retinal space. Right, en face SS-OCTA projection of the outer retina and the corresponding flow density map in a 3 × 3 mm field of the LE demonstrating hyperintense signal due to flow within an inactive lesion (vascularized disciform scar). Note the much less vessel density represented by a faint yellow color code compared to the RE signal intensity. The quality of SS-OCTA image of the LE is degraded by motion artifacts due to poor fixation. Corresponding SS-OCT shows the hyper-reflective lesion in the sub-retinal space.

a distinct active neovascular complex which appeared as a small tuft of bright high-flow (hyperintense signal) curvilinear vessels, whereas SS-OCTA of the LE at the plane of the outer retina demonstrated flow within inactive lesion (vascularized disciform scar). It is worth noting that in this case, both FFA and SS-OCT were inconclusive in confirming the diagnosis and the state of activity of CNV; meanwhile, SS-OCTA unequivocally displayed active CNV in the RE and vascularized disciform scar in the LE (**Figures 11** and **12**).

8. Limitations of SS-OCTA in imaging macular dystrophies

Despite the obvious advantages of OCTA as a noninvasive risk-free technology, an important consideration is that a sizeable portion of the population, targeted by OCTA imaging in macular dystrophies, is in the pediatric age group. Often, children are unable to maintain steady fixation during OCTA examination; hence, the quality of the image could be degraded by motion artifacts and segmentation errors. Future advances in eye tracking and segmentation algorithms, and introduction of portable machines for examination under anesthesia could improve the versatility of OCTA technology in imaging macular dystrophies.

9. Conclusion

The appearance of clinical changes on fundus examination of patients with macular dystrophies is synonymous with the already established damage of a certain level with consequent visual morbidity. Until the present date, OCTA has proven its efficacy in imaging macular dystrophies and identifying the morphological alteration in the vascular layers of the ocular fundus associated with different disease stages. Moreover, SS-OCTA is an essential imaging tool whenever FFA and SS-OCT reveal inconclusive results in the advent of CNV development secondary to vitelliform macular dystrophy. The future of OCTA in imaging macular dystrophies lies in its potential for screening target population and identifying patients at incipient disease stages well in advance of visible clinical changes by depicting specific OCTA pattern or OCTA *signature* that is diagnostic for a particular macular dystrophy. The objective is to identify patients who would be best candidates for the ongoing trials on gene therapy and stem cell transplantation before irreversible visual dysfunction sets in.

Author details

Magdy Moussa[1,2]* and Mahmoud Leila[3]

*Address all correspondence to: magdymoussa60@gmail.com

1 Ophthalmology Department, Faculty of Medicine, Tanta University, Tanta, Egypt

2 MEDIC Eye Center, Tanta, Egypt

3 Retina Department, Research Institute of Ophthalmology, Giza, Egypt

References

[1] Sohn EH, Mullins RF, Stone EM. Macular dystrophies. In: Ryan SJ, editor. Retina. 5th ed. Philadelphia: Saunders; 2013. pp. 852-886

[2] Agarwal A, JDM G. Heredodystrophic disorders affecting the pigment epithelium and retina. In: Gass' Atlas of Macular Diseases. 5th ed. Philadelphia: Saunders; 2012. pp. 239-436

[3] Richard G, Soubrane G, Yannuzzi LA. Hereditary disorders. In: Fluorescein and ICG Angiography. Textbook and Atlas. 2nd ed. New York: Thieme; 1998. pp. 200-225

[4] von Rückman A, Fitzke FW, Bird AC. Distribution of fundus autofluorescence with a scanning laser ophthalmoscope. The British Journal of Ophthalmology. 1995;**79**(5):407-412

[5] Delori FC, Dorey CK, Staurenghi G, Arend O, Goger DG, Weiter JJ. In vivo fluorescence of the ocular fundus exhibits retinal pigment epithelium lipofuscin characteristics. Investigative Ophthalmology & Visual Science. 1995;**36**(3):718-729

[6] Delori F, Greenberg JP, Woods RL, Fischer J, Duncker T, Sparrow J, Smith RT. Quantitative measurements of autofluorescence with the scanning laser ophthalmoscope. Investigative Ophthalmology & Visual Science. 2011;**52**:9379-9390

[7] Greenberg JP, Duncker T, Woods RL, Smith RT, Sparrow JR, Delori FC. Quantitative fundus autofluorescence in healthy eyes. Investigative Ophthalmology & Visual Science. 2013;**54**:5684-5693

[8] Burke TR, Duncker T, Woods RL, et al. Quantitative fundus autofluorescence in recessive Stargardt disease. Investigative Ophthalmology & Visual Science. 2014;**55**:2841-2852

[9] Duncker T, Lee W, Tsang SH, et al. Distinct characteristics of inferonasal fundus autofluorescence patterns in stargardt disease and retinitis pigmentosa. Investigative Ophthalmology & Visual Science. 2013;**54**:6820-6826

[10] Smith RT, Gomes NL, Barile G, et al. Lipofuscin and autofluorescence metrics in progressive STGD. Investigative Ophthalmology & Visual Science. 2009;**50**:3907-3914

[11] Khan KN, Kasilian M, Mahroo OAR, Tanna P, Kalitzeos A, Robson AG, Tsunoda K, Iwata T, Moore AT, Fujinami K, Michaelides M. Early patterns of macular degeneration in ABCA4–Associated retinopathy. Ophthalmology. 2018;**125**(5):735-746

[12] Rezaei KA, Zhang Q, Chen CL, Chao J, Wang RK. Retinal and choroidal vascular features in patients with retinitis pigmentosa imaged by OCT based microangiography. Graefe's Archive for Clinical and Experimental Ophthalmology. 2017;**255**:1287-1295

[13] Adhi M, Read SP, Ferrara D, Weber M, Duker JS, Waheed NK. Morphology and vascular layers of the choroid in Stargardt disease analyzed using spectral-domain optical coherence tomography. American Journal of Ophthalmology. 2015;**160**(6):1276-1284

[14] Giani A, Pellegrini M, Carini E, Peroglio Deiro A, Bottoni F, Staurenghi G. The dark atrophy with indocyanine green angiography in Stargardt disease. Investigative Ophthalmology & Visual Science. 2012;**53**(7):3999-4004

[15] Mastropasqua R, Toto L, Borrelli E, Di Antonio L, Mattei PA, Senatore A, Di Nicola M, Mariotti C. Optical coherence tomography angiography findings in Stargardt disease. PLoS One. 2017;**12**(2):e0170343. DOI: 10.1371/journal.pone.0170343

[16] Guduru A, Lupidi M, Gupta A, Jalali S, Chhablani J. Comparative analysis of autofluorescence and OCT angiography in Stargardt disease. The British Journal of Ophthalmology. 2017;**0**:1-4. DOI: 10.1136/bjophthalmol-2017-311000

[17] Korte GE, Reppucci V, Henkind P. RPE destruction causes choriocapillary atrophy. Investigative Ophthalmology & Visual Science. 1984;**25**(10):1135-1145

[18] Neuhardt T, May CA, Wilsch C, Eichhorn M, Lutjen-Drecoll E. Morphological changes of retinal pigment epithelium and choroid in rd-mice. Experimental Eye Research. 1999; **68**(1):75-83

[19] Blaauwgeers HG, Holtkamp GM, Rutten H, et al. Polarized vascular endothelial growth factor secretion by human retinal pigment epithelium and localization of vascular endothelial growth factor receptors on the inner choriocapillaris. Evidence for a trophic paracrine relation. The American Journal of Pathology. 1999;**155**:421-428

[20] Stanga PE, Tsamis E, Papayannis A, Stringa F, Cole T, Jalil A. Swept-source optical coherence tomography angiography™ (Topcon Corp, Japan): Technology review. Developments in Ophthalmology. 2016;**56**:13-17

[21] Bonnin S, Mané V, Couturier A, Julien M, Paques M, Tadayoni R, Gaudric A. New insight into the macular deep vascular plexus imaged by optical coherence tomography angiography. Retina. 2015;**35**:2347-2352

[22] Grulkowski I, Liu JJ, Potsaid B, Jayaraman V, Lu CD, Jiang J, Cable AE, Duker JS, Fujimoto JG. Retinal, anterior segment and full eye imaging using ultrahigh speed swept source OCT with vertical-cavity surface emitting lasers. Biomedical Optics Express. 2012;**3**:2733-2751

[23] Gao SS, Liu G, Huang D, Jia Y. Optimization of the split-spectrum amplitude-decorrelation angiography algorithm on a spectral optical coherence tomography system. Optics Letters. 2015;**40**:2305-2308

[24] Kuehlewein L, Tepelus TC, An L, Durbin MK, Srinivas S, Sadda SR. Noninvasive visualization and analysis of the human parafoveal capillary network using swept source OCT optical microangiography. Investigative Ophthalmology & Visual Science. 2015;**56**: 3984-3988

[25] Savastano MC, Lumbroso B, Rispoli M. In vivo characterization of retinal vascularization morphology using optical coherence tomography angiography. Retina. 2015;**35**: 2196-2203

[26] Pechauer AD, Jia Y, Liu L, Gao SS, Jiang C, Huang D. Optical coherence tomography angiography of peripapillary retinal blood flow response to hyperoxia. Investigative Ophthalmology & Visual Science. 2015;**56**:3287-3291

[27] Sambhav K, Grover S, Chalam KV. The application of optical coherence tomography angiography in retinal diseases. Survey of Ophthalmology. 2017;**62**:838-866

[28] De Carlo TE, Adhi M, Salz DA, Joseph T, Waheed NK, Seddon JM, Duker JS, Reichel E. Analysis of choroidal and retinal vasculature in inherited retinal degenerations using optical coherence tomography angiography. Ophthalmic Surgery, Lasers & Imaging Retina. 2016;**47**:120-127

[29] Parodi MB, Cicinelli MV, Rabiolo A, Pierro L, Bolognesi G, Bandello F. Vascular abnormalities in patients with Stargardt disease assessed with optical coherence tomography angiography. The British Journal of Ophthalmology. 2017;**101**:780-785

[30] Querques G, Zambrowski O, Corvi F, Miere A, Semoun O, Srour M, Souied EH. Optical coherence tomography angiography in adult-onset foveomacular vitelliform dystrophy. The British Journal of Ophthalmology. 2016;**100**:1724-1730

[31] Parodi MB, Rabiolo A, Cicinelli MV, Iacono P, Romano F, Bandello F. Quantitative analysis of optical coherence tomography angiography in adult-onset foveomacular vitelliform dystrophy. Retina. 2018;**38**:237-244

[32] Parodi MB, Romano F, Cicinelli MV, Rabiolo A, Arrigo A, Pierro L, Iacono P, Bandello F. Retinal vascular impairment in best vitelliform macular dystrophy assessed by means of optical coherence tomography angiography. American Journal of Ophthalmology. 2018;**187**:61-70

[33] Lupidi M, Coscas G, Cagini C, Coscas F. Optical coherence tomography angiography of a choroidal neovascularization in adult onset foveomacular vitelliform dystrophy: Pearls and pitfalls. Investigative Ophthalmology & Visual Science. 2015;**56**:7638-7645

[34] Guduru A, Gupta A, Tyagi M, Jalali S, Chhablani J. Optical coherence tomography angiography characterization of best disease and associated choroidal neovascularization. The British Journal of Ophthalmology. 2018;**102**:444-447

[35] Treder M, Lauermann JL, Alnawaiseh M, Heiduschka P, Eter N. Quantitative changes in flow density in patients with adult-onset foveomacular vitelliform dystrophy: An OCT angiography study. Graefe's Archive for Clinical and Experimental Ophthalmology. 2018;**256**:23-28

[36] Demirel S, Yanık Ö, Nalcı H, Batıoğlu F, Özmert E. The use of optical coherence tomography angiography in pachychoroid spectrum diseases: A concurrent comparison with dye angiography. Graefe's Archive for Clinical and Experimental Ophthalmology. 2017;**255**:2317-2324

[37] Tan ACS, Tan GS, Dennsiton AK, Keane PA, Ang M, Milea D, Chakravarthy U, Cheung CMG. An overview of the clinical applications of optical coherence tomography angiography. Eye. 2018;**32**:262-286

[38] El-Maftouhi MQ, El Maftouhi A, Eandi CM. Chronic central serous chorioretinopathy imaged by optical coherence tomographic angiography. American Journal of Ophthalmology. 2015;**160**(3):581-587.e1

[39] Moussa M, Leila M, Khalid H, Lolah M. Detection of silent type I choroidal neovascular membrane in chronic central serous chorioretinopathy using en face swept-source optical coherence tomography angiography. Journal of Ophthalmology. 2017; Article ID 6913980:1-10. doi.org/10.1155/2017/6913980

[40] Moussa M, Leila M. Swept-source optical coherence tomography angiography in pediatric patients. European Ophthalmology News. 09.2016.XXXIV congress of the ESCRS report